LAWRENCE
LIVERMORE
NATIONAL
LABORATORY

UCRL-JRNL-207542

Time-Resolved Single-State Measurements of the Electronic Structure of Isochoric Heated Copper

A. J. Nelson, J. Dunn, K. Widmann, T. Ao, Y. Ping, J. Hunter, A. Ng

October 28, 2004

Applied Physics Letters

UCRL-JRNL- 207542

Time-Resolved Single-State Measurements of the Electronic Structure of Isochoric Heated Copper

A.J. Nelson[1], J. Dunn[2], K. Widmann[2], T. Ao[3], Y. Ping[2], J. Hunter[2] and A. Ng[2,3]
[1]Chemistry & Materials Science Directorate, Lawrence Livermore National Laboratory, Livermore, CA 94551
[2]Physics & Advanced Technologies Directorate, Lawrence Livermore National Laboratory, Livermore, CA 94551
[3]Department of Physics & Astronomy, University of British Columbia, Vancouver, B.C., Canada

Time-resolved x-ray photoelectron spectroscopy is used to probe the non-steady-state evolution of the valence band electronic structure of laser heated ultra-thin (50 nm) Cu. Single-shot x-ray laser induced time-of-flight photoelectron spectroscopy with picosecond time resolution is used in conjunction with optical measurements of the disassembly dynamics that have shown the existence of a metastable liquid phase in *fs*-laser heated Cu foils persisting 4-5 ps. This metastable phase is studied using a 527 nm wavelength 400 fs laser pulse containing 0.1 – 2.5 mJ laser energy focused in a large 500 x 700 μm^2 spot to create heated conditions of 0.07 – 1.8 x 10^{12} W cm^{-2} intensity. Valence band photoemission spectra showing the changing occupancy of the Cu 3*d* level with heating are presented. These are the first picosecond x-ray laser time-resolved photoemission spectra of laser-heated ultra-thin Cu foil showing changes in electronic structure. The ultrafast nature of this technique lends itself to true single-state measurements of shocked and heated materials.

Electron-phonon coupling and the subsequent electron-ion equilibration govern the ultrafast evolution of the electronic structure of a material under nonequilibrium conditions. Thermalization of the electrons stimulated by the electric field of an ultrafast laser pulse is a nonequilibrium process that is still not well understood. Time-resolved x-ray diffraction experiments have been applied to characterize ultrafast laser-induced changes in the atomic structure of melting surfaces and show that below a given threshold laser fluence, the primary mechanism of energy transfer between hot carriers and the lattice is coherent acoustic phonon generation via deformation potential coupling and longitudinal-optical phonon decay. [1-5] In addition, time-resolved x-ray absorption measurements of changes in the electronic structure of laser heated Si has shown the existence of a transient liquid phase before vaporization and before disassembly. [6]

Photoelectron spectroscopy is one of the preferred techniques for probing the static electronic structure of materials and is now applicable to the dynamic regime with picosecond time resolution using various excitation sources. Specifically, results from the investigations on metals have shown that ultrafast laser heating affects changes in the electron energy distribution. [7-9] In addition, time-resolved Si 2p core-level photoemission reveals that electrons become mobile as the bulk solid phase changes to an intermediate metallic fluid phase. [10] Another example implements a high harmonic generation (HHG) extreme ultraviolet (EUV) source coupled with a time-of-flight (ToF) spectrometer for pump-probe experiments. These studies have included semiconductor electron population dynamics as well as monitoring the surface chemical reaction of molecular oxygen and CO on Pt(111) with femtosecond time resolution. [11,12] These higher order harmonic sources have the advantage of shorter duration since the process is

driven by ultrafast laser pulses, e.g. less than 60 fs, at a high repetition rate which makes them very attractive for dynamic pump-probe experiments. However, the presence of multiple harmonics requires further wavelength selection with multilayer-coated optics or a wavelength dispersive element and the lower photon fluence/shot requires multiple shots to achieve good signal statistics. The line width of a single harmonic is still wide and dictated by the spectral width of the laser drive.

In this Letter, we describe our optical pump - x-ray laser induced time-of-flight photoelectron spectroscopy probe technique and show results on the investigation of changes in the electronic structure of Cu undergoing ultrafast isochoric laser heating. The ultra-thin Cu target consists of 50 nm Cu on a 20 nm C support. The pulsed x-ray laser source has several characteristics that are very important to the time-of-flight technique that include picosecond duration, highly monochromatic single line, high degree of coherence and sufficient photon fluence to record a complete photoelectron spectrum in a single shot. [13-15]

The Ni-like Pd ion 4*d* – 4*p* soft x-ray laser line at 14.7 nm (84.5 eV) is generated by two 1054 nm wavelength pump beams of the Lawrence Livermore National Laboratory Compact Multipulse Terawatt (COMET) laser source [16]. This tabletop x-ray laser typically requires 5 J of laser pump energy and fires at a rate of 1 shot every 4 minutes. High x-ray photon numbers ($>10^{12}$/shot), in a highly monochromatic line ($E/\Delta E \sim 4 – 5 \times 10^4$), and with short ~2 – 5 ps (FWHM) pulse duration have been measured for this source [17,18]. When combined with small source area and beam divergence properties of the 14.7 nm line this gives ultra-high peak brightness ~ $10^{24} – 10^{25}$ ph. mm^{-2} mrad^{-2} s^{-1} (0.1% BW) $^{-1}$. Overall, the 14.7 nm peak brightness is 5 – 6 orders of

magnitude higher than 3rd generation synchrotron undulator sources. However, these undulator sources still have higher average brightness of $0.5 – 6 \times 10^{18}$ ph.mm^{-2} mrad^{-2} s^{-1} (0.1% BW)$^{-1}$ at 50 – 10 nm, respectively.

Figure 1 shows a schematic of the x-ray laser photoelectron spectroscopy experimental setup. The x-ray laser probe is collimated by a normal incidence Mo:Si multilayer spherical mirror and relayed along the beamline by a 45° Mo:Si multilayer flat mirror. The narrow reflectivity window of the mirrors selects the x-ray laser wavelength and minimizes other plasma x-rays reaching the sample. A pinhole or thin filter isolates the beamline from the experimental ultra-high vacuum (UHV) chamber, operating below 10^{-8} Torr. The x-ray laser is aligned using a back-thinned CCD camera to a cross wire fiducial on the sample manipulator. A fast 400 fs (FWHM), 527 nm wavelength laser pump beam can be focused and aligned similarly to overlap the two beams onto the sample. The optical pump laser is timed relative to the x-ray laser beam at the sample to within ~5 ps. The pump beam produces rapid heating and depending on the intensity can excite bound electrons, induce phase changes or ionize the sample. The x-ray laser beam can probe the material at various times generating the photoelectrons from the sample surface. Low energy photoelectrons, with K.E. < 84.5 eV, emitted from the valence band and shallow core levels are detected by the modified e-ToF spectrometer, the operation of which is described in detail elsewhere. [19] The signal is acquired and digitized using a fast 1.5 GHz oscilloscope.

The disassembly dynamics of the laser heated ultra-thin Cu foil were investigated to determine the lifetime of intermediate states during ultrafast heating. Changes in the optical properties and the dynamic behavior of the heated foil were monitored using

Frequency Domain Interferometry (FDI). [20,21] This diagnostic measures the change in phase shift, $\delta\phi$, of the 150-fs (FWHM), 800-nm probe reflected off the front surface of the foil which was heated by a 150-fs (FWHM), 400-nm pump pulse at an intensity of 3 – 5 X 10^{12} W/cm^2. $\delta\phi$ is sensitive to both the dielectric function and hydrodynamic expansion of the heated material. By varying the relative time delay between the 400-nm pump and the 800-nm probe, we were able to determine the onset of target disassembly as shown in Figure 2. Note that the 800 nm probe and 400 nm pump wavelengths are below and above the interband absorption threshold, respectively, for Cu. [22] Also, for reference, the 1/e penetration depth of 2ω light (400 nm, 3.10 eV) in Cu is 14.9 nm. Furthermore, the ballistic electron range in Cu is 70 nm, thus resulting in a uniformly heated 50 nm thin Cu slab for these experiments. The FDI measurements show the existence of a metastable liquid phase in the *fs*-laser-heated ultra-thin Cu foils persisting for approximately 4-5 ps (hatched area in Figure 2). Similar results have been observed for Au and Al. [23] The persistence of this single state for several picoseconds allow us to accurately probe the dynamic conditions of the foil with picosecond duration x-rays.

Figure 3 presents the single-shot e-ToF photoemission spectra of the 3*d* valence band of static and laser heated ultra-thin polycrystalline Cu foil illuminated with 10^8 – 10^9 x-ray laser photons. This sample is sufficiently thin to observe the transmitted x-ray laser beam simultaneously with the photoelectron signal. The x-ray prompt peak seen in the spectrum with no drift voltage is generated from scattered x-rays off the Cu foil surface hitting the micro-channel plate (MCP) detector a distance of L = 43.75 cm away. [19] The x-ray prompt peak occurs L/c = 1.46 ns after the x-ray laser hits the sample, where c is the speed of light, and can be used as a timing fiducial. Since the mean escape

depth of the photoemitted electrons is on the order of ~5-10 Å for this kinetic energy, the spectrum should be more indicative of a Cu-oxide layer in the absence of sputter ion cleaning. In addition, the photoelectron yield as given by $N_p = F\sigma n\lambda T$ can be estimated from the x-ray fluence on the sample after filter and mirror losses ($F = 10^9$ photons/pulse), the Cu 3*d* photoionization cross-section ($\sigma \approx 8.712 \times 10^{-18}$ cm^2) [24], the Cu number density ($n = 8.4 \times 10^{22}$ cm^{-3}), the escape depth ($\lambda = 5 \times 10^{-8}$ cm), and the angular collection efficiency of the MCP detector ($T = 2.5 \times 10^{-4}$). Therefore, we can expect 9.1×10^3 photoelectrons/pulse to arrive at the MCP detector and produce signal. We observe single-shot photoelectron signals in the range of 2-4 V without the application of a retarding field.

Under static conditions the 3*d* valence band electrons will have the highest kinetic energies as governed by $E_k = h\nu - E_b - \phi$, where $h\nu$ is the energy of the incident photon (84.5 eV), E_b is the binding energy of the photoelectron relative to the Fermi level and ϕ is the work function of the material (ϕ = 4.6 eV for Cu)**.** Also, the photoionization cross-section for the Cu 3*d* shell at excitation energy of 80 eV is 8.712 Mb. [24] Valence band photoemission will thus be the first and strongest event in the e-ToF spectrum. The strong Cu *d*-state emission observed at the valence band maximum, i.e. first e-ToF event, is indicative of a high density of states (filled *d*-states) that are 2 eV below the Fermi level. [22, 25] The strong emission corresponds to direct transitions from *d*-like occupied bands to unoccupied bands above the Fermi energy. The initial as well as the final states determine the appearance, position, and intensity of these structures, and strongly depend on the applied photon energy. Non-equilibrium perturbations of the valence band states created by the x-ray laser intensity (10^7 W/cm^2) also contribute to the unusually abrupt

electron energy distribution at the valence band edge. Displaying the ambient x-ray laser induced Cu valence band photoemission spectrum versus kinetic energy (Figure 4) yields an energy distribution curve that is qualitatively comparable to Cu valence band photoemission spectra presented in the literature [26] that were acquired using synchrotron radiation.

The experiment was repeated again with the 400 fs, 527 nm (2.35 eV) optical pump beam focused onto a large 500 × 700 μm^2 (FWHM) spot on the ultra-thin (50 nm) polycrystalline Cu foil. Note that the optical pump energy is above the interband absorption threshold and has a 1/e penetration depth in Cu of 16.2 nm. The x-ray laser probe and optical pump were timed to coincide on the sample. Two laser heating conditions were applied (1) 300 μJ of laser energy corresponding to 2×10^{11} W cm^{-2} intensity and (2) 2.49 mJ of laser energy corresponding to 1.8×10^{12} W cm^{-2} intensity. It is noted that the x-ray laser beam overfilled the optical beam on the sample so that there are detected photoelectron signals from heated and unheated regions of the foil.

The single-shot e-ToF photoemission spectra of the 3*d* valence band of the laser heated ultra-thin polycrystalline Cu foil (Figs. 3 and 4) clearly show that the observed 3*d* peak intensity decreases with increasing laser energy and that there exist features before the strong onset that represents the valence band maximum. The decreasing Cu 3*d* peak intensity is due to a depopulation of the *d*-band as the electron temperature T_e increases. [27-29] Depopulation of the valence band *d* states also creates vacancies in the conduction band (CB) thus allowing interband absorption below the edge (e.g., 3*d*-4*p* transitions in Cu). In addition, we observe that the Cu 3*d* peak shifts towards lower kinetic energy (higher binding energy) indicating that the band is 'sinking'. Depopulation

of the *d*-band is predicted to affect its binding energy in this manner. [28,29] Also, note that there is no broadening of the Cu 3*d* upon heating which implies a nonequilibrium distribution of occupied states i.e. smearing of the Fermi-Dirac electron energy distribution. Increasing the pump energy by a further factor of ten generates a strong electron signal before 50 ns (Fig. 3) that indicates the sample is in an ionized state. Also, note the two prompt peaks separated by 2 ns, that we attribute to multiple scattering of the incident x-rays during skin layer expansion and ablation of the Cu.

In summary, we have successfully demonstrated the optical pump-x-ray laser probe characterization capability to observe the evolution of changes in the electronic structure of laser heated ultra-thin Cu with picosecond time resolution. The first preliminary measurements of the disassembly dynamics of fs-laser heated ultra-thin Cu foil were also performed. Single-shot spectra have been achieved showing that the incident photon number is more than enough for characterizing dynamical events. The dynamic pump-probe results reveal depopulation of the Cu *d*-band and a smearing of the Fermi-Dirac electron energy distribution. We will further investigate and characterize the range of x-ray laser intensities on the sample and the effect of space charge on the nonequilibrium electron energy distribution in future studies.

This work was performed under the auspices of the U.S. Department of Energy by the University of California Lawrence Livermore National Laboratory under Contract No. W-7405-Eng-48.

References

1. A. H. Chin, R.W. Schoenlein, T. E. Glover, P. Balling, W. P. Leemans, and C. V. Shank, Phys. Rev. Lett. **83**, 336 (1999).
2. C.W. Siders, A. Cavalleri, K. Sokolowski-Tinten, Cs. Toth, T. Guo, M. Kammler, M. Horn von Hoegen, K. R. Wilson, D. von der Linde, C. P. J. Barty, Science **286**, 1340 (1999).
3. Christoph Rose-Petruck, R. Jimenez, T. Guo, A. Cavalleri, C. W. Siders, F. Raksi, J. A. Squier, B. C. Walker, K. R. Wilson & C. P. J. Barty, Nature **398**, 310 (1999).
4. A.M. Lindenberg, I. Kang, S.L. Johnson, T. Misalla, P.A. Heimann, Z. Chang, J. Larsson, P.H. Bucksbaum, H.C. Kapteyn, H.A. Padmore, R.W. Lee, J.S. Wark, and R.W. Falcone, Phys. Rev. Lett. **84**, 111 (2000).
5. K. Sokolowski-Tinten, C. Blome, J. Blums, A. Cavalleri, C. Dietrich, A. Tarasevitch, I. Uschmann, E. Förster, M. Kammler, M. Horn-von-Hoegen, and D. von der Linde, Nature **422**, 287 (2003).
6. S. L. Johnson, P. A. Heimann, A.M. Lindenberg, H.O. Jeschke, M. E. Garcia, Z. Chang, R.W. Lee, J. J. Rehr, and R.W. Falcone, Phys. Rev. Lett. **91**, 157403 (2003).
7. W.S. Fann, R. Storz, and J. Bokor, Phys. Rev. **B44**, 10980 (1991).
8. W.S. Fann, R. Storz, H.W.K. Tom and J. Bokor, Phys. Rev. Lett. **68**, 2834 (1992).
9. P. Oelhafen, R. Wahrenberg and H. Stupp, J. Phys. Condens. Matter **12**, A9 (2000).
10. T. E. Glover, G. D. Ackerman, A. Belkacem, P. A. Heimann, Z. Hussain, R.W. Lee, H. A. Padmore, C. Ray, R.W. Schoenlein, W. F. Steele, and D. A. Young, Phys. Rev. Lett. **90**, 236102 (2003).
11. M. Bauer, C. Lei, K. Read, R. Tobey, J. Gland, M. M. Murnane, and H. C. Kapteyn,

Phys. Rev. Lett. **87(2)**, 025501-1 (2001).

12. G. Tsilimis, C. Benesch, J. Kutzner, and H. Zacharias, J. Opt. Soc. Am. **B20**, 246 (2003).
13. A.J. Nelson, J. Dunn, T. van Buuren, J. Hunter, R.F. Smith, O. Hemmers, and D.W. Lindle, *Soft X-Ray Lasers and Applications V*, ed. E.E. Fill et al, SPIE Proceedings **5197**, 168 (2003).
14. J. Dunn, R.F. Smith, J. Nilsen, A.J. Nelson, T. Van Buuren, S.J. Moon, J.R. Hunter, J. Filevich, J.J. Rocca, M.C. Marconi, V.N. Shlyaptsev, *X-Ray Lasers 2002: 8th International Conference on X-ray Lasers*, ed. J.J. Rocca et al, AIP Conference Proceedings No. **641**, 481 (2002).
15. A.J. Nelson, J. Dunn, T. van Buuren, J. Hunter, Appl. Phys. Lett. **85** (2004). *In press*
16. J. Dunn, Y. Li, A. L. Osterheld, J. Nilsen, J. R. Hunter, and V. N. Shlyaptsev, Phys. Rev. Lett. **84**, 4834 (2000).
17. R.F. Smith, J. Dunn, J. R. Hunter, J. Nilsen, S. Hubert, S. Jacquemot, C. Remond, R. Marmoret, M. Fajardo, P. Zeitoun, L. Vanbostal, C. L.S. Lewis, M. Francoise Ravet, F. Delmotte, Opt. Lett. 28(22), 2261 (2003).
18. J. Dunn *et al.*, *Soft x-ray lasers and Applications V*, SPIE Int. Soc. Opt. Eng. Proc, vol. **5197**, ed. E.E. Fill and S. Suckewer, 51-59 (2003).
19. O. Hemmers, S.B. Whitfield, P. Glans, H. Wang, D.W. Lindle, R. Wehlitz, and, I.A. Sellin, Rev. Sci. Instrum. **69**, 3809 (1998).
20. J.P. Geindre, P. Audebert, A. Rousse, F. Falliès, J.C. Gauthier, A. Mysyrowicz, A. Dos Santos, G. Hamoniaux, and A. Antonetti, Opt. Lett. **19**, 1997 (1994).

21. K.Widmann, G. Guethlein, M.E. Foord, R.C. Cauble, F.G. Patterson, D.F. Price, F.J. Rogers, P.T. Springer, R.E. Stewart, A. Ng, T. Ao, A. Forsman, Phys. Plasmas **8**, 3869 (2001).

22. J.F. Janak, A.R. Williams and V.L. Moruzzi, Phys. Rev. **B11**, 1522 (1975).

23. K. Widmann, T. Ao, M. E. Foord, D. F. Price, A. D. Ellis, P. T. Springer, and A. Ng, Phys. Rev. Lett. **92**, 125002 (2004).

24. J.-J. Yeh and I. Lindau, "Atomic Subshell Photoionization Cross Sections and Asymmetry Parameters: $1 \leq Z \leq 103$", *Atomic Data and Nuclear Data Tables* 32, 11 (1985).

25. N. Smith, Phys. Rev. **B3**, 1862 (1971).

26. J. Stöhr, F.R. McFeely, G. Apai, P.S. Wehner and D.A. Shirley, Phys. Rev. **B14**, 4431 (1976).

27. P.B. Johnson and R.W. Christy, Phys. Rev. **B11**, 1315 (1975).

28. D.F. Price, R.M. More, R.S. Walling, G. Guethlein, R.L. Shepherd, R.E. Stewart, W.E. White, Phys. Rev. Lett. **75**, 252 (1995).

29. D. Fisher, M. Fraenkel, Z. Zinamon, Z. Henis, E. Moshe, Y. Horovitz, E. Luzon, S. Maman and S. Eliezer, *28th European Conference on Laser Interaction with Matter*, Rome (2004).

Figure Captions

Figure 1. Schematic of the optical pump – x-ray laser induced time-of-flight photoemission probe of material surfaces.

Figure 2. Temporal behavior of the relative phase shift ($\delta\Phi$) of the 800-nm probe pulse reflected off the isochorically heated ultra-thin Cu slab. The hatched area indicates the existence of a metastable liquid phase.

Figure 3. X-ray laser induced photoelectron spectra (signal versus time-of-flight) for static and laser heated ultra-thin polycrystalline Cu foil.

Figure 4. X-ray laser induced photoelectron spectra (signal versus kinetic energy) for static and laser heated ultra-thin polycrystalline Cu foil.

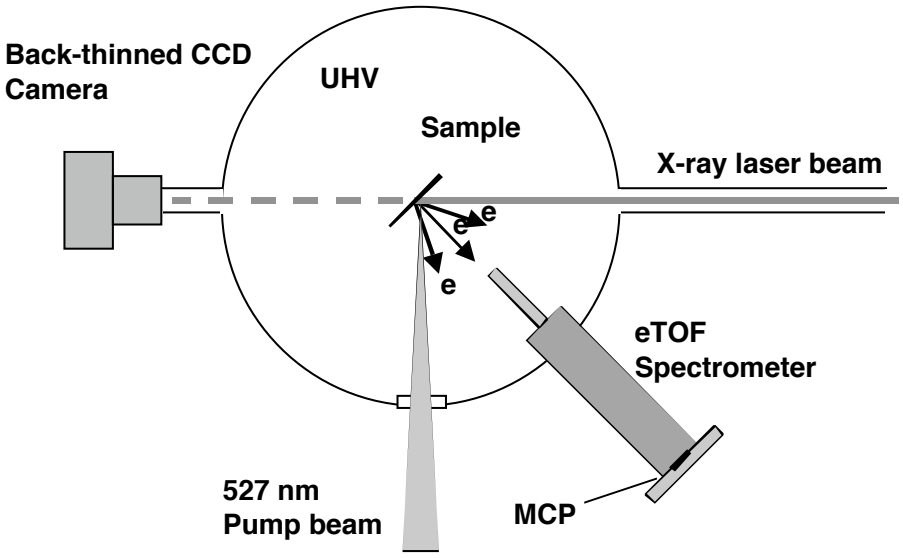
Back-thinned CCD
Camera
UHV
Sample
X-ray laser beam
e
e
e
eTOF
Spectrometer
527 nm
Pump beam
MCP

Figure 1.

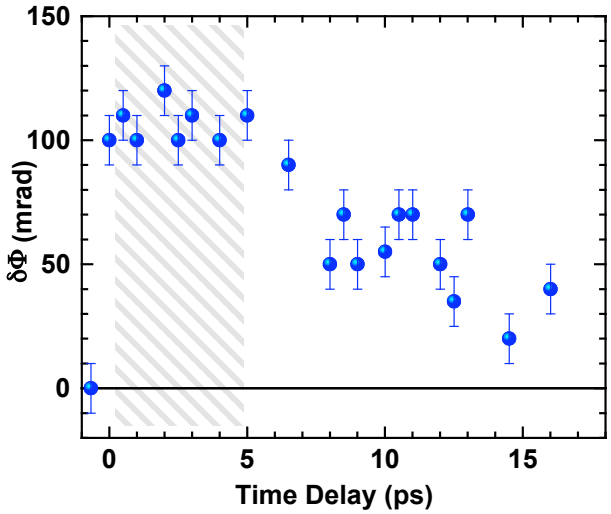

Figure 2.

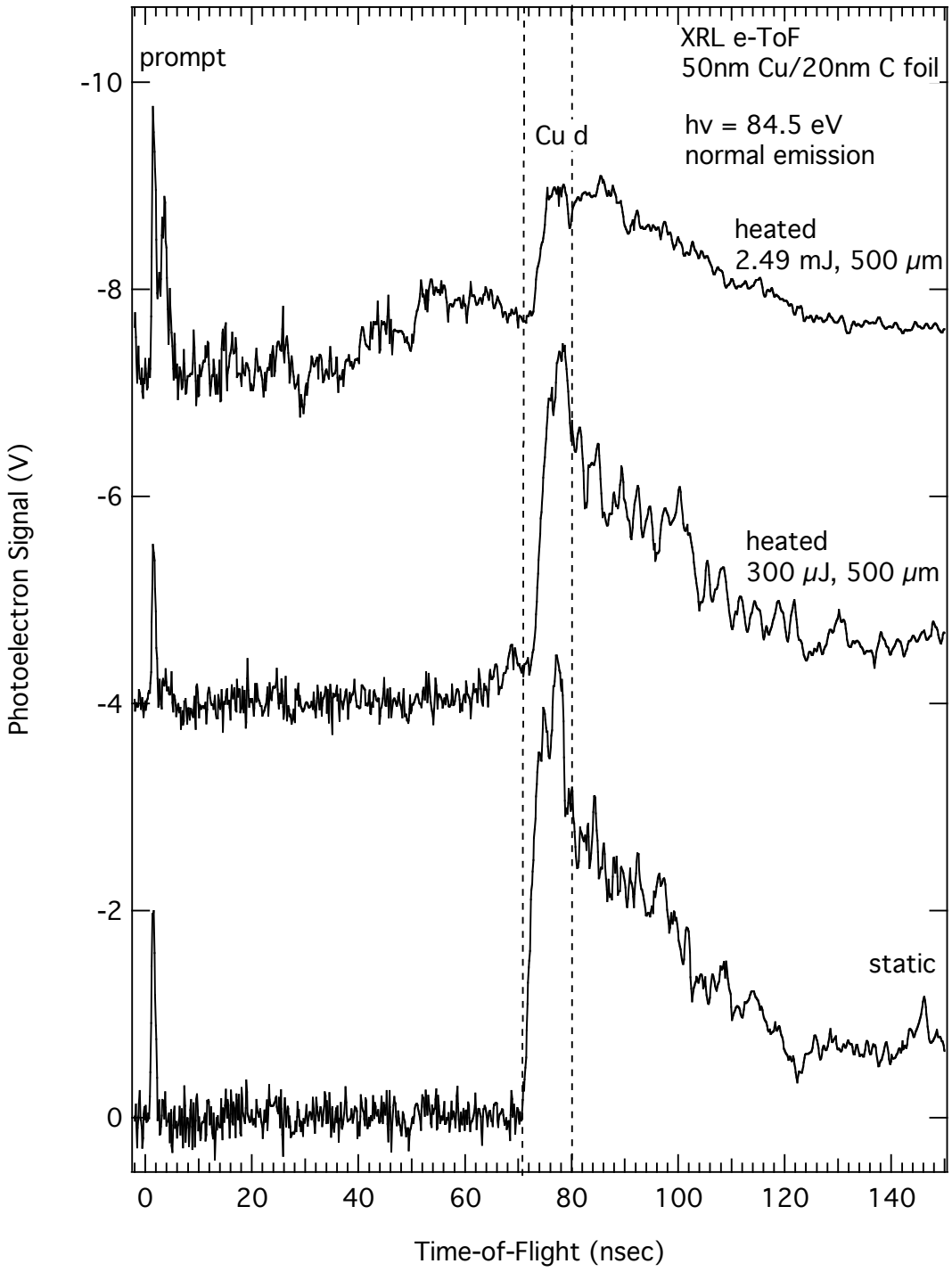
prompt
XRL e-ToF
50nm Cu/20nm C foil
hv = 84.5 eV
normal emission
Cu d
heated
2.49 mJ, 500 μm
heated
300 μJ, 500 μm
static
Photoelectron Signal (V)
-10
-8
-6
-4
-2
0
0
20
40
60
80
100
120
140
Time-of-Flight (nsec)

Figure 3.

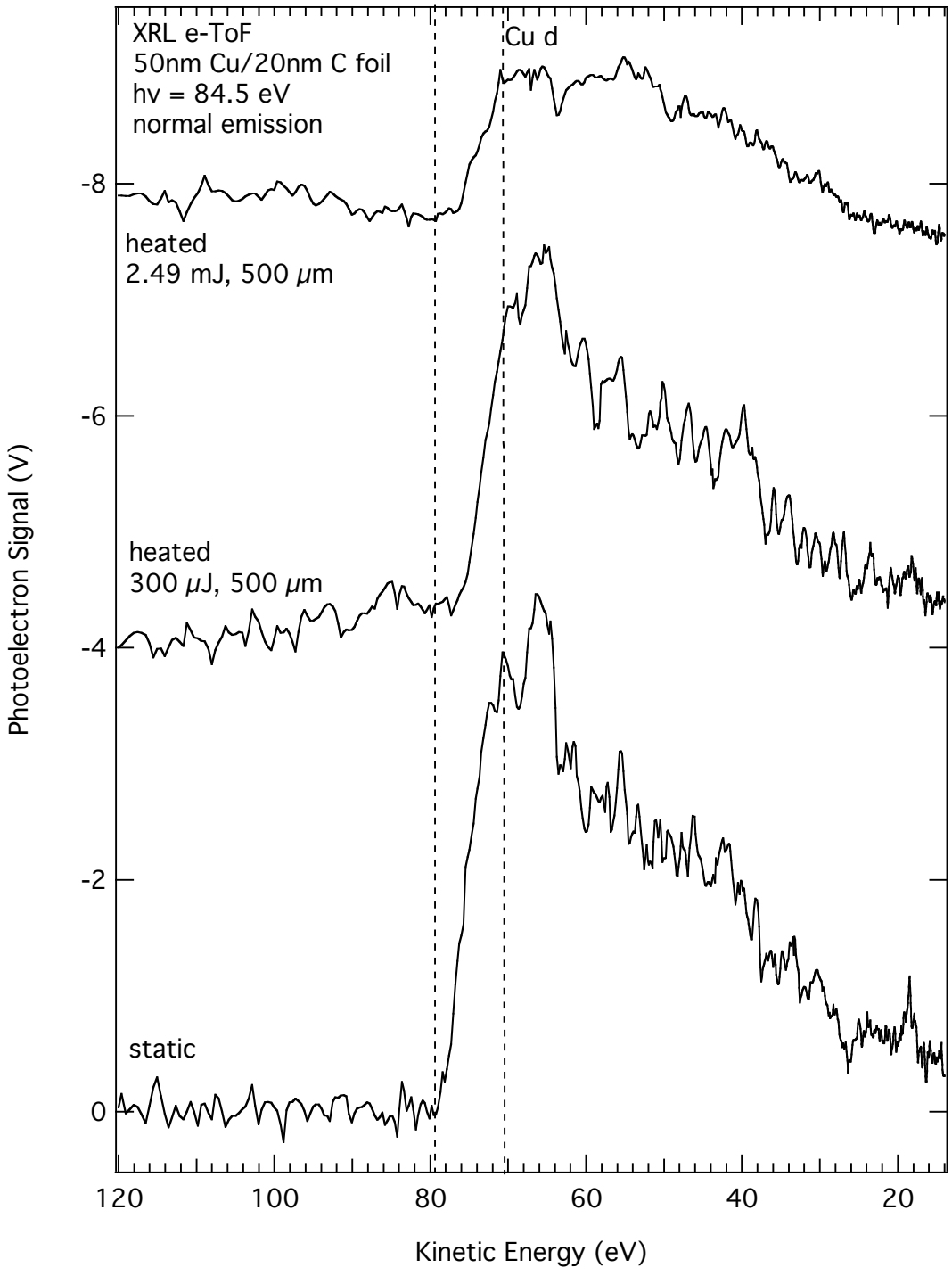
XRL e-ToF
50nm Cu/20nm C foil
hv = 84.5 eV
normal emission
Cu d
heated
2.49 mJ, 500 μm
heated
300 μJ, 500 μm
static
Photoelectron Signal (V)
-8
-6
-4
-2
0
120
100
80
60
40
20
Kinetic Energy (eV)

Figure 4.